TRACE ELEMENT DISTRIBUTION AND IMPLICATIONS IN SEDIMENTS ACROSS THE ALLERØD–YOUNGER DRYAS BOUNDARY IN THE NETHERLANDS AND BELGIUM

ALEXANDRE V. ANDRONIKOV[1,2], ANNELIES VAN HOESEL[3], IRINA E. ANDRONIKOVA[2] and WIM Z. HOEK[4]

[1]Lunar and Planetary Laboratory, University of Arizona, Tucson, AZ, USA
[2]Division of Geochemistry and Laboratories, Czech Geological Survey, Prague, Czech Republic
[3]Leiden University, Faculty of Archaeology, Leiden, The Netherlands
[4]Utrecht University, Faculty of Geoscience, Utrecht, The Netherlands

Andronikov, A.V., Van Hoesel, A., Andronikova, I.E. and Hoek, W.Z., 2016. Trace element distribution and implications in sediments across the Allerød–Younger Dryas boundary in the Netherlands and Belgium. *Geografiska Annaler: Series A, Physical Geography*, 00, 1–21. DOI:10.1111/geoa.12140

ABSTRACT. In the Northern Hemisphere, the Younger Dryas cooling occurred between 12.8 and 11.7 ka BP. This cooling is thought to have been the result of an abrupt change in atmospheric and oceanic circulations. One of the hypotheses explaining such a change suggests that just before the onset of the Younger Dryas cooling, multiple airbursts/impacts occurred over the Northern Hemisphere. We studied the late Pleistocene sediments from the Netherlands and Belgium to check whether a sudden short event might have taken place just before the onset of the Younger Dryas cooling. The geochemical features revealed suggest that such events might have occurred. The presence of products of biomass burning is suggested on the basis of trace element features of sediments from the lower Younger Dryas boundary. The presence of a volcanic component and a component resulting from extensive biomass burning in the sediments of *c*. 12.9 ka BP are indicated on the basis of trace element features. The volcanic component may be related to the Laacher See volcano eruption, whereas the cause of the extensive biomass burning remains unclear.

Key words: geochemistry, late Pleistocene sediments, trace elements

Introduction

In the Northern Hemisphere, the cold period known as the Younger Dryas climate oscillation occurred between *c*. 12.8 ka BP and *c*. 11.7 ka BP (e.g. Peteet 1995; Alley 2000; Björck 2007; Lowe *et al.* 2008; Kennett *et al.* 2015). This climate change is generally thought to result from an abrupt change of atmospheric and oceanic circulations (e.g. Berger 1990; Teller *et al.* 2002; McManus *et al.* 2004; Brauer *et al.* 2008; Murton *et al.* 2010; Rayburn *et al.* 2011). Among other hypotheses on the origin of the Younger Dryas cooling, is the one proposed by Firestone *et al.* (2007). This hypothesis in its original form suggests that a large bolide exploded over the North American Laurentide Ice Sheet *c*. 12.8 ka BP and that the consequences of this event triggered the onset of Younger Dryas cooling. In its present state, the Younger Dryas Impact Hypothesis suggests that a major cosmic episode of multiple airbursts/impacts occurred at 12,800 ± 300 calibrated years BP (see Kennett *et al.* 2015 and references therein). Most pros and cons of this *extraterrestrial* (*ET*) hypothesis are considered in detail in Pinter *et al.* (2011), Bunch *et al.* (2012), Israde-Alcántara *et al.* (2012), Wittke *et al.* (2013), van Hoesel (2014) and van Hoesel *et al.* (2014, 2015). If the impact occurred over North America, moreover, if this was a broadly distributed multiple impact event, transportation of the impact-related microparticles eastward by the dominating move of the air masses from west to east could have delivered such particles as far to the east as West and East Europe (cf. Brauer *et al.* 2008; Muhs *et al.* 2010). Some studies showed that in the Late Pleistocene sediments of Western Europe, material which could be related to ET impact is present (see Israde-Alcántara *et al.* 2012). In order to search for geochemical fingerprints of short and possibly catastrophic events during the time

DOI:10.1111/geoa.12140

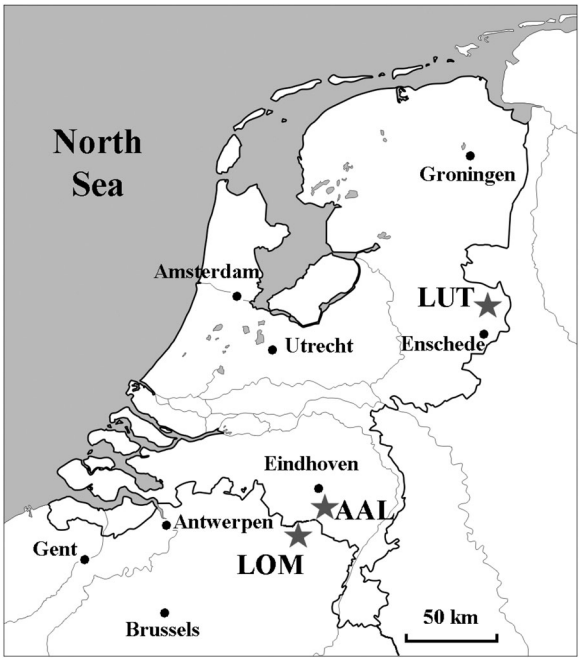

Fig. 1. A map showing location of the studied sites (AAL, Geldrop-Aalsterhut; LOM, Lommel; LUT, Lutterzand).

transitional from the Allerød to Younger Dryas, in some cases, the onset of the Allerød–Younger Dryas boundary in Europe is clearly visible as a marked organic-rich and often charcoal-bearing Usselo horizon. We studied geochemistry of the late Glacial sediments, where the Usselo Horizon was originally described (Hijszeler 1957), from a few well dated localities in the Netherlands and NE Belgium. These areas are located in the type region of the Younger Dryas cool episode, traditionally used as global stratigraphic reference sites These regions were also selected because there are several reports on the presence of possible impact-related markers (nanodiamonds and microspherules) in sediments from the Lommel Maatheide site in NE Belgium (Tian *et al.* 2010; Wittke *et al.* 2013). In this paper, we present the results of *laser ablation inductively coupled plasma mass spectrometer* (*LA-ICP-MS*) analyses of sediments from the Allerød–Younger Dryas transition at Geldrop-Aalsterhut and Lutterzand sites in the Netherlands, and Lommel Molse-Nete and Lommel Maatheide sites in Belgium (Fig. 1). The results are used to check whether any geochemical signatures in sediments of West Europe may support the impact hypothesis of Firestone *et al.* (2007).

Methods

Sampling strategy

All field sites sampled are located within the European sand belt, which forms continuous aeolian deposits occurring along the vast territory from the Netherlands to Western Russia (e.g. Kasse 2002; Bertran *et al.* 2009; Kaiser *et al.* 2009). In the studied areas, the late-Glacial part of these deposits is represented by aeolian Younger Coversand I (deposited during the Older Dryas stadial) and Younger Coversand II (deposited during the Younger Dryas stadial). In between (mostly during the warmer Allerød interstadial), soil formation on top of the higher and dryer parts of the Younger Coversand I led to the formation of a soil variety of the Usselo Horizon, whereas thin peat layers of the Usselo Horizon developed in lower wetter areas (e.g. Kasse 2002; Kaiser *et al.* 2009). Stratigraphically, the Allerød–Younger Dryas boundary is located within the Usselo Horizon. All sites sampled include either the soil or the peat variety of the Usselo Horizon.

Geldrop-Aalsterhut

Geldrop-Aalsterhut is a site in late Pleistocene sediments, which is located along the E25 highway

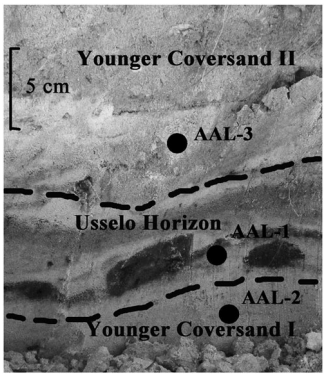

Fig. 2. A studied part of the late Pleistocene sedimentary sequence at the Geldrop-Aalsterhut site. The Usselo Horizon is characterized by the presence of areas rich in charcoal (black spots). The sampling spots are shown.

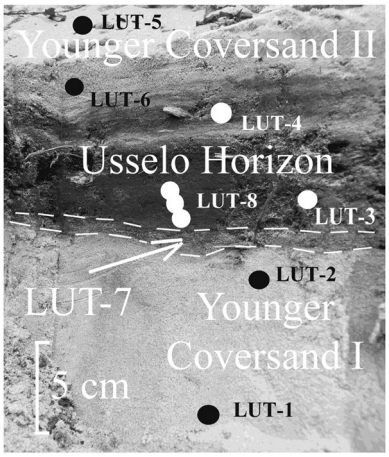

Fig. 3. A studied part of the late Pleistocene sedimentary sequence at the Lutterzand site. A thin sandy layer (LUT-7) between the Younger Coversand I and the Usselo Horizon is marked. The sampling spots are shown.

in the southern part of the Netherlands, 5 km south of the city of Eindhoven (de Vries *et al.* 1958). The sediments here are represented by sands of the Younger Coversand I (yellow and bleached sand), with the Usselo Horizon (a thin charcoal-rich layer above the bleached horizon) atop of it (Fig. 2). The Usselo Horizon is covered by sand dunes of the Younger Coversand II (yellowish loamy sand). Stratigraphy of this site was studied in detail by van Hoesel *et al.* (2012) and van Hoesel (2014) who dated charcoal from the Usselo Horizon at this location by the *accelerator mass spectrometry* (*AMS*) radiocarbon method and provided 12 785–12 650 *calibrated* (*cal*) years BP ages. The sampled upper part of the Younger Coversand I is AMS radiocarbon dated to 13 080–12 915 cal years BP, and the sampled lower part of the Younger Coversand II is dated by the same method as varying between 12 700 and 12 585 cal years BP [see van Hoesel *et al.* (2012) and van Hoesel (2014), and references therein]. We collected three samples from the Geldrop-Aalsterhut site (outcrop AAL) (Fig. 2).

Lutterzand

Multiple outcrops of the late Pleistocene sediments are located along the eastern banks of the Dinkel River in the easternmost part of the Netherlands close to the German border (15 km northeast of the city of Enschede). The sediments here are represented by the Younger Coversand I (horizontally laminated, loamy, fine light-yellow sands) and the Younger Coversand II (horizontally laminated, loamy yellow sands), separated by the Usselo Horizon (either soil or a peat layer; e.g. Bateman and van Huissteden 1999; Bateman 2008) (Fig. 3). The outcrop we studied is described in detail in Vandenberghe *et al.* (2013; profile 1). In that study, the peat layer was AMS radiocarbon dated to 10 480 ± 70 ^{14}C years BP (12 560–12 240 cal years BP), which corresponds to the Younger Dryas period. Both underlying and overlying sediments were dated by *optically simulated luminescence* (*OSL*) to 13.8 ± 1.1 ka BP (average of six measurements) and 12.7 ± 0.9 ka BP (average of two measurements), respectively (Vandenberghe *et al.* 2013). Eleven samples altogether were collected from the outcrop (LUT samples) containing a 5–10 cm peat-rich layer of the Usselo Horizon (Fig. 3).

Lommel Molse-Nete

This site is located in NE Belgium near the city of Lommel. The studied late Pleistocene sediments (Fig. 4) are represented by the Younger Coversand I (its upper part transitional from yellow sand to bleached sand), with the Usselo Horizon (the bleached layer topped by a thin charcoal-bearing part) atop of it, and by the Younger Coversand II (by its lower part represented by yellowish loamy sand) covering the Usselo Horizon. The stratigraphy of this site was studied in detail by Vanmontfort *et al.* (2010a, 2010b). Three charcoal samples from the Usselo Horizon were dated to an average 11 480 ± 35 ^{14}C years BP [13 495–13 165 cal years BP; from van Hoesel *et al.* (2014) recalibrated using IntCal09] that corresponds to the Allerød

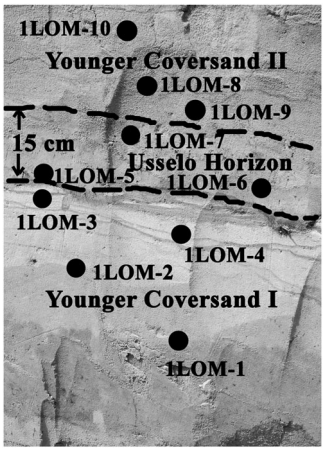

Fig. 4. A studied part of the late Pleistocene sedimentary sequence at the Lommel Molse-Nete site. The Usselo Horizon contains rare small charcoal fragments, which are not seen in the picture. The sampling spots are shown.

period. The radiocarbon dating of samples from a closely located and stratigraphically very similar Arendonk-Korhaan site gives ages from 13 300 cal years BP to 12 800 cal years BP for the Younger Coversand I, and from 12 900 cal years BP to 12 400 cal years BP for the Younger Coversand II (Derese *et al.* 2012). Ten samples altogether were collected from the Lommel Molse-Nete site (1LOM samples) (Fig. 4).

Lommel Maatheide

The outcrop is located ~10 km NW from Lommel Molse-Nete on the territory of the former zinc smelter factory (Horckmans *et al.* 2006). The studied sediments are represented by the Younger Coversand I (its upper part is bleached) and by the Younger Coversand II (yellowish loamy sand) separated by a peat layer of ~40 cm thick (Fig. 5) grading into a bleached horizon with charcoal particles dispersed (an incomplete and eroded Usselo Horizon). A charcoal sample from the Usselo Horizon has been radiocarbon dated to 11 480 ± 100 ^{14}C years BP (13 435–13 245 cal years BP; Wittke *et al.* 2013). Overall, three profiles of the Lommel Maatheide outcrop cover the age interval from *c.* 13.5 ± 0.9 ka (average of four measurements) to *c.* 11.3 ± 0.8 ka BP (average of two measurements) (Derese *et al.* 2012; OSL dating). We collected 15 samples altogether from three profiles (2LOM, 2A-LOM, and 2B-LOM) along the outcrop stretching for ~50 m (see Derese *et al.* 2012 for detailed stratigraphy). Three samples were collected from the profile 2LOM (Fig. 5a), six samples were collected from the profile 2A-LOM (Fig. 5b*)*, and six more samples were collected from the profile 2B-LOM (Fig. 5c).

Sample preparation and analytical techniques

Each sedimentary sample was dried, pulverized, and resulted powders were pressed to pellets of 1 cm diameter. Samples of charcoal from sediments of the Netherlands and France were picked from the host sand, mounted in epoxy and slightly polished to achieve a flat surface. Much bigger fragments of charcoal from modern wood fires in Arizona were slightly polished to achieve flat surfaces and then were mounted in modeling clay. The samples were analyzed for trace elements at the University of Arizona. A CETAC UV Nd:YAG LXS-213 laser coupled with a ThermoFinnigan Element2 ICP-MS was used for analysis. The laser was operated in a six-spot rastering mode with three analytical runs per sample for higher representativity of the bulk sample composition. During the analytical runs, the laser beam was focused onto the sample surface with 150-μm-diameter spot, the laser was operated at 50% maximum energy output (see Table 1 for analytical parameters), with 300 laser shots per a spot. The He carrier gas was mixed with the Ar carrier gas flow upline of the plasma torch. A NIST SRM-612 silicate glass standard and a pellet made from the International Association of Geoanalysts SdAR-1 material (enhanced river sand; Webb, P.C., Thompson, M., Potts, P.J. and Wilson, S., unpubl.) were used as references (Sylvester and Eggins 1997; Jochum *et al.* 2011; Andronikov *et al.* 2013). Analyses were run in the low mass resolution mode of the instrument (i.e. M/ΔM of about 300). Iron57 was used as an internal standard (concentrations of Fe were independently analyzed in solutions by ICP-MS for sample 1MS10-01 from the Earp Marl, and for the International Association of Geoanalysts SdAR-1; Webb, P.C., Thompson, M., Potts, P.J. and Wilson, S., unpubl.). We analyzed samples of the Late Pleistocene (Allerød) Earp Marl from Murray Springs, Arizona (USA), which are older than the time of the ET impact suggested by Firestone *et al.* (2007), and by no means can be influenced by such an impact. Repeated analyses of the standards (after each unknown sample) ensured that all results are consistent and comparable. The measurements were based on integrated multi-element time-resolved signals.

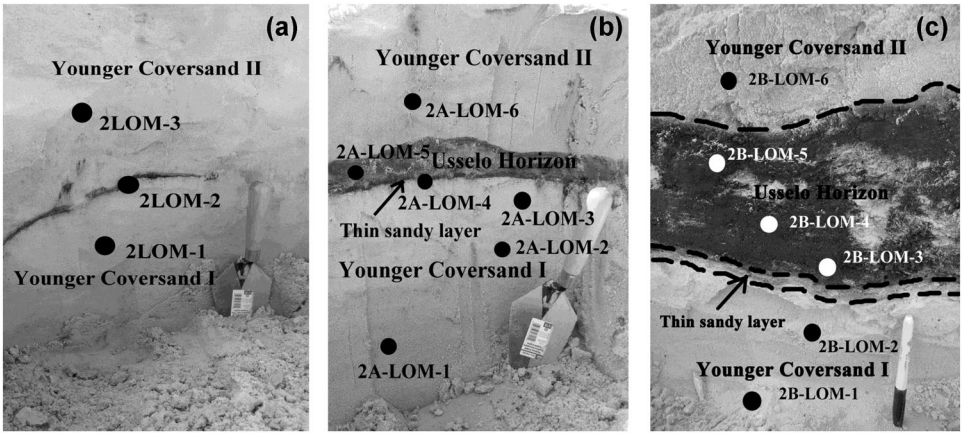

Fig. 5. A studied part of the Late Pleistocene sedimentary sequence at the Lommel Maatheide site: (a) a profile of 2LOM; (b) a profile of 2A-LOM; (c) a profile of 2B-LOM. The site is characterized by the presence of a thin layer of grayish sand at the very basis of the peat-rich Usselo Horizon. The sampling spots are shown.

Because of overall very low *platinum group elements* (*PGE*) concentrations in terrestrial sediments, it is impossible to get PGE concentrations reliably using the laser ablation method for bulk analysis of terrestrial sedimentary samples. However, since we tried in this study only to recognize features of the PGE behavior for different samples, and not precise PGE concentrations, we analyzed samples only in order to compare PGE signal intensities on the ICP-MS spectra for different samples. Samples of PGE signal intensities were normalized to the Earp Marl signal intensities for consistency of the analytical results.

One of the challenges in determination of trace elements in natural samples with LA-ICP-MS is the influence of the "matrix effect", i.e. the composition and physical properties of the standards should be as close to those of the analyzed sample as possible (e.g. Jochum *et al.* 2007; Sylvester 2008). To overcome the influence of the "matrix effect", we used two references: one is the NIST612 glass standard (Sylvester and Eggins 1997; Jochum *et al.* 2011), and the other is a pellet made from the pulverized International Association of Geoanalysts SdAR-1 material (with physical properties and composition close to those of the analyzed samples; Webb, P.C., Thompson, M., Potts, P.J. and Wilson, S., unpubl.). Repeated analyses of the NIST612 standard and the SdAR-1 material (after every three runs of the unknown samples) ensured that all results are consistent and comparable. Cross determinations of composition of the reference materials (Table 2) showed that the laser ablation technique provides high-quality results for most trace elements. Because there is no reliable reference material for trace element concentrations in charcoal, all the information presented on the composition of charcoal samples should be considered preliminary. Nevertheless, since we are interested only in the behavior of trace elements relative to each other for the purposes of the present study, the results obtained for the charcoal samples are sufficient and are considered in detail in the "Discussion".

Table 1. Instrumental parameters

Element 2 ICP-MS	
Sample gas flow	1.05 L min^{-1}
Auxiliary gas flow	0.85 L min^{-1}
Coolant gas flow	15.7–16.7 L min^{-1}
Forward power	1200 W
Reflected power	1–3 W
Cones	Al
CETAC LSX-213 Laser ablation unit	
Sample gas flow (Ar)	1.20 L min^{-1}
Carrier gas flow (He)	0.71 L min^{-1}
Laser output energy (100%)	4 mJ $pulse^{-1}$
Laser repetition rate	20 Hz

Analytical results

Geldrop-Aalsterhut

The sample AAL-2 from the Younger Coversand I is depleted (up to two times) in Ti, Zr, Hf, Ta, Nb, and Mn compared with the sample AAL-3 (Younger Coversand II), whereas concentrations of other trace elements are similar for both samples (Table 3). The sample AAL-1 from the charcoal-bearing sandy Usselo Horizon displays

Table 2. Results of cross-analyses of the applied reference materials (ppm)

	LOD (ppm)	SdAR-1, Webb *et al.* (2012)[a]	NIST-612, Jochum *et al.* (2011)	Composition of SdAR-1 after NIST-612	2σ	Composition of NIST-612 after SdAR-1	2σ
No. of analyses				16		16	
P	4	698	46.6	706	102	43.6	6.0
S	15	n.d.	377	1300	98	n.d.	
Sc	0.08	8.2	39.9	8.6	0.42	41.1	3.6
Ti	1.0	3765	44.0	3810	123	43.8	2.8
V	0.4	68.27	38.8	68.3	2.9	39.0	3.0
Cr	0.7	92.7	36.4	162	14.8	38.2	3.5
Mn	0.5	5405	38.7	5642	378	38.3	2.8
Fe	6.0	32375	51.0	32204	1530	54.0	7.8
Co	0.9	10.71	35.5	10.9	0.62	36.2	2.0
Ni	0.5	40.80	38.8	40.6	1.8	38.2	2.1
Cu	0.05	302	37.8	36.8	2.2	40.0	2.1
Zn	0.05	932.1	39.1	40.2	3.0	39.7	2.0
Rb	0.02	142.8	31.4	31.4	1.8	31.6	1.6
Sr	0.1	151.5	78.4	78.8	2.9	79.8	2.6
Y	0.20	40.90	38.3	37.2	2.4	38.8	2.2
Zr	0.25	352.8	37.9	342	16.0	38.2	2.2
Nb	0.05	34.70	38.9	37.6	2.2	39.9	2.4
La	0.16	58.25	36.0	59.2	2.8	36.1	1.9
Ce	0.05	110.9	38.4	104.2	5.3	39.1	1.8
Pr	0.03	12.55	37.9	13.2	0.52	38.0	2.0
Nd	0.2	46.08	35.5	45.4	1.6	35.7	1.3
Sm	0.05	8.525	37.7	8.8	0.40	37.4	1.8
Eu	0.04	1.338	35.6	1.31	0.06	36.0	1.4
Gd	0.3	7.500	37.3	8.24	0.62	38.1	2.4
Tb	0.03	1.213	37.6	1.29	0.06	37.3	1.4
Dy	0.07	7.315	35.5	7.43	0.42	35.8	2.0
Ho	0.04	1.480	38.3	1.52	0.12	38.3	2.4
Er	0.16	4.326	38.0	4.40	0.24	38.3	2.4
Tm	0.02	0.662	36.8	0.664	0.04	36.6	1.6
Yb	0.06	4.280	39.2	42.0	0.20	39.1	1.8
Lu	0.02	0.669	37.0	0.656	0.04	37.2	2.1
Hf	0.04	n.d.	36.7	3.68	0.16	n.d.	
Ta	0.01	2.202	37.6	2.54	0.12	37.4	1.6
W	0.06	10.29	38.0	10.8	0.68	37.9	2.0
Pb	0.09	979.3	38.57	960	24	38.4	1.6
Th	0.01	17.97	37.79	18.5	0.78	37.6	1.4
U	0.01	4.277	37.38	4.62	0.32	37.2	1.8

[a] Webb, P.C., Thompson, M., Potts, P.J. and Wilson, S., unpubl.

The following isotopes were monitored during the analytical runs: P^{31}, S^{34}, Sc^{45}, Ti^{47}, V^{51}, Cr^{53}, Mn^{55}, Fe^{57}, Co^{59}, Ni^{60}, Cu^{65}, Zn^{66}, Rb^{85}, Sr^{88}, Y^{89}, La^{139}, Ce^{140}, Pr^{141}, Nd^{143}, Sm^{147}, Eu^{153}, Gd^{157}, Tb^{159}, Dy^{163}, Ho^{165}, Er^{166}, Tm^{169}, Yb^{172}, Lu^{175}, Hf^{178}, Ta^{181}, W^{182}, Pb^{208}, Th^{232}, and U^{238}.

LOD, limit of detection (ppm); n.d., no data available.

concentrations of Zr, Hf, Ta, Nb, and Mn comparable to or higher than those in the overlaying sample AAL-3, and much higher concentrations of the REE than in both Younger Coversand samples (Table 3). Trace element patterns normalized to the *average continental crust* (*ACC*; Wedepohl 1995) show that Nb-Ta, P, Sr, Zr-Hf, Ti, and Co-Ni form deep troughs for the Usselo Horizon sample (Fig. 6). A trough at Nb-Ta is also visible for a sample from Younger Coversand II, and troughs at P and Sr are observed for all samples. The PGE signals on the ICP-MS spectra for the Geldrop-Aalsterhut samples are low, however being mostly above the Arizona marl level (Table 4).

Lutterzand

Sediments of Younger Coversands I (LUT-1 and LUT-2) and II (LUT-5 and LUT-6) display similar concentrations to most trace elements. Only concentrations of Co and Ni are significantly higher in the Younger Coversand II than in the

Table 3. Chemical composition of Late Pleistocene sediments from the Geldrop-Aalsterhut, Lutterzand and Lommel sites (ppm)

	Geldrop-Aalsterhut			Lutterzand				
	AAL-1	AAL-2	AAL-3	LUT-1	LUT-2	LUT-3	LUT-4	LUT-5
P	111.1	172.7	213.9	631.3	312.8	1218	1124	585.6
S	346.1	357.3	483.4	1012	900.4	15410	8158	619.2
Sc	48.55	23.39	33.91	95.89	52.20	42.38	56.94	37.52
Ti	2332	2721	4107	7590	6228	6087	8262	3445
V	69.32	105.2	167.0	260.3	163.8	120.4	188.4	130.6
Cr	62.40	50.96	125.0	402.3	133.7	337.1	570.8	197.8
Mn	201.7	327.6	460.3	159.4	101.1	155.8	270.5	13.29
Co	6.612	8.530	15.06	34.88	14.19	11.09	17.83	31.15
Ni	22.83	12.64	24.28	38.95	34.30	54.76	86.18	84.13
Cu	27.00	17.38	29.68	19.09	20.56	46.68	93.86	11.90
Zn	4444	1050	8523	8907	579.3	4512	8878	726.8
Rb	155.5	148.4	202.6	409.4	274.5	n.d.	n.d.	226.4
Sr	52.06	31.40	50.50	85.28	65.67	n.d.	n.d.	77.79
Y	30.43	5.731	7.216	9.786	23.18	n.d.	n.d.	7.342
Zr	115.1	117.7	315.7	276.6	61.51	255.2	402.6	85.98
Nb	16.58	16.24	23.98	19.70	16.23	52.35	33.94	21.77
La	143.4	22.19	44.4	32.86	28.85	311.9	733.1	18.83
Ce	117.4	63.24	95.35	90.61	52.99	436.1	260.2	83.74
Pr	14.62	4.052	4.964	7.749	6.846	64.28	33.31	4.844
Nd	54.92	13.47	13.85	15.68	16.91	267.7	143.4	12.44
Sm	18.15	4.119	3.641	6.201	4.397	71.88	44.60	6.102
Eu	3.789	0.874	0.964	1.008	0.975	16.32	9.434	1.038
Gd	15.90	3.452	3.755	5.403	7.096	85.27	39.91	2.864
Tb	2.120	0.533	0.490	0.355	0.566	14.29	7.273	0.360
Dy	12.30	2.875	2.452	2.140	4.093	75.98	44.36	2.007
Ho	2.200	0.425	0.598	0.345	0.844	15.75	8.204	0.525
Er	6.047	1.340	1.458	1.848	2.611	43.31	20.59	1.238
Tm	1.060	0.236	0.357	0.202	0.464	5.723	3.311	0.304
Yb	7.305	1.970	3.949	1.429	2.136	35.44	18.70	1.275
Lu	0.654	0.148	0.241	0.160	0.247	4.614	2.067	0.145
Hf	1.674	2.693	6.854	6.328	1.592	5.946	7.631	2.033
Ta	0.822	0.946	1.354	0.952	1.423	3.100	2.458	1.200
W	2.226	3.010	3.822	4.044	2.726	1.870	3.634	4.159
Pb	47.04	61.88	85.67	107.9	36.40	55.61	47.80	26.71
Th	7.655	4.638	7.096	6.008	6.318	29.17	29.46	11.09
U	3.251	3.429	5.634	4.511	3.387	8.890	8.907	6.164

	Lutterzand					Lommel Molse-Nete		
	LUT-6	LUT-7	LUT8-1	LUT8-2	LUT8-3	1LOM-1	1LOM-2	1LOM-3
P	591.9	263.5	447.5	1113	719.4	1334	927.8	841.7
S	729.1	6535	13146	45131	31891	633.7	519.2	624.6
Sc	31.27	65.81	40.93	38.66	46.05	39.27	35.69	23.36
Ti	5206	3950	3950	3870	5586	4166	3993	4705
V	191.0	172.5	119.8	222.6	194.8	263.2	211.0	235.2
Cr	263.8	358.2	303.4	521.9	389.1	147.8	96.03	99.68
Mn	15.29	317.5	163.3	158.6	216.8	404.2	478.6	472.8
Co	40.97	22.40	12.43	23.55	15.45	14.09	12.02	17.35
Ni	94.22	298.1	48.35	120.9	80.81	19.47	13.69	13.36
Cu	7.995	60.06	51.27	104.5	57.34	10.59	7.506	7.778
Zn	1299	3098	1587	1545	4988	421.1	281.3	154.4
Rb	240.3	n.d.	n.d.	n.d.	n.d.	359.5	288.1	291.5
Sr	98.25	n.d.	n.d.	n.d.	n.d.	55.07	36.42	37.51
Y	14.62	n.d.	n.d.	n.d.	n.d.	12.57	5.347	6.908
Zr	190.3	636.6	269.6	359.9	582.5	581.9	85.36	168.6
Nb	34.68	31.21	34.16	51.00	53.81	30.20	21.44	26.56
La	56.95	345.8	134.5	654.2	871.5	39.45	10.36	23.19
Ce	120.8	440.3	185.0	706.4	980.5	75.42	77.58	79.60

Continued

Table 3. Continued

	Lutterzand					Lommel Molse-Nete		
	LUT-6	LUT-7	LUT8-1	LUT8-2	LUT8-3	1LOM-1	1LOM-2	1LOM-3
Pr	10.18	92.78	29.21	97.59	183.0	5.366	4.374	5.473
Nd	27.10	381.8	122.0	370.1	710.4	22.21	15.09	17.68
Sm	7.080	104.9	35.08	83.72	162.3	5.172	2.210	3.186
Eu	2.061	22.78	7.911	18.97	36.47	0.902	0.555	0.656
Gd	10.03	114.3	36.04	108.9	171.1	3.992	2.305	3.002
Tb	0.771	20.86	6.656	19.25	35.81	0.500	0.298	0.317
Dy	4.025	112.0	32.30	101.7	206.4	2.188	2.392	1.621
Ho	0.884	21.21	6.318	22.47	42.19	0.610	0.536	0.297
Er	1.840	53.07	16.50	57.57	116.3	1.483	0.838	0.886
Tm	0.487	7.745	2.344	8.425	14.49	0.357	0.173	0.179
Yb	2.964	44.44	14.50	47.35	81.00	2.140	1.253	1.031
Lu	0.300	5.010	1.843	6.699	11.51	0.247	0.094	0.119
Hf	4.773	8.036	6.630	8.853	13.27	10.71	2.645	4.843
Ta	2.208	3.197	2.655	6.021	4.306	1.567	1.069	1.446
W	6.851	3.860	4.708	4.843	5.313	7.449	3.720	3.839
Pb	56.64	2484	2509	78.22	76.66	101.2	76.08	76.60
Th	17.37	22.87	24.21	37.27	50.45	9.375	7.026	12.30
U	8.442	8.491	6.389	14.44	13.19	9.045	5.594	5.281

	Lommel Molse-Nete						
	1LOM-4	1LOM-5	1LOM-6	1LOM-7	1LOM-8	1LOM-9	1LOM-10
P	649.8	1272	679.5	1288	1692	1399	1362
S	500.5	505.7	295.9	1078	949.8	743.3	828.4
Sc	62.57	40.66	22.47	84.10	58.90	120.1	51.51
Ti	4324	6985	4391	5357	4644	3787	3715
V	186.1	317.7	167.6	387.0	345.4	238.9	275.6
Cr	108.8	208.4	130.3	408.0	299.7	180.6	229.1
Mn	537.7	334.7	153.8	452.3	556.6	1501	1994
Co	14.18	29.37	11.12	26.91	58.22	17.34	52.72
Ni	12.51	62.16	44.89	216.8	136.9	71.09	114.2
Cu	7.321	35.71	18.90	31.89	18.66	14.61	25.49
Zn	1545	3278	1223	5210	653.1	2573	3124
Rb	297.2	272.0	167.0	344.5	316.2	172.6	312.3
Sr	40.32	55.79	37.06	92.17	56.16	53.20	56.42
Y	8.142	14.36	11.29	45.31	7.226	16.23	10.03
Zr	153.9	793.5	232.6	437.9	126.4	359.9	228.1
Nb	25.87	29.44	19.80	36.08	20.46	20.29	24.40
La	33.14	213.0	28.67	143.2	26.77	25.66	22.41
Ce	63.50	138.5	168.3	183.2	124.1	129.3	150.4
Pr	5.807	7.538	3.578	19.81	4.781	5.861	7.961
Nd	15.70	21.33	9.040	59.95	12.92	17.34	21.05
Sm	3.246	6.324	3.145	17.52	2.288	4.993	4.763
Eu	0.720	1.573	0.810	3.720	0.746	1.659	1.157
Gd	2.896	8.583	4.11	14.05	3.647	7.606	5.366
Tb	0.384	0.928	0.368	2.474	0.369	0.625	0.902
Dy	2.404	5.611	2.108	14.88	1.378	2.852	3.084
Ho	0.378	1.160	0.413	2.618	0.305	0.576	0.901
Er	1.238	3.359	0.893	6.349	0.977	1.525	2.052
Tm	0.233	0.835	0.337	0.810	0.230	0.311	0.346
Yb	1.472	5.024	1.733	5.657	1.044	1.886	2.102
Lu	0.182	0.577	0.156	0.609	0.107	0.222	0.286
Hf	4.831	29.54	3.931	7.778	3.033	10.49	5.143
Ta	1.525	2.213	1.144	2.448	1.167	1.194	1.749
W	4.475	5.321	2.322	6.946	4.133	2.847	4.163
Pb	82.73	101.4	86.20	138.6	90.94	62.68	123.7
Th	7.359	18.91	8.175	29.77	11.16	14.13	17.24
U	5.925	7.734	12.93	9.354	5.276	6.486	8.875

Continued

Table 3. Continued

	Lommel Maatheide							
	2LOM-1	2LOM-2	2LOM-3	2A-LOM1	2A-LOM2	2A-LOM3	2A-LOM4	2A-LOM5
P	57.69	302.3	317.2	96.00	71.98	196.7	663.8	907.0
S	524.4	1179	670.8	388.2	247.9	614.0	1670	15702
Sc	12.12	110.4	36.50	11.74	15.65	18.27	54.17	34.19
Ti	1700	6781	3578	377.2	308.9	2272	9784	2271
V	27.91	298.6	90.88	42.04	22.00	30.23	460.0	126.5
Cr	36.29	243.4	113.8	62.71	29.88	47.90	376.4	385.8
Mn	32.65	244.4	63.07	17.41	2.659	47.23	297.5	288.5
Co	3.658	20.73	11.38	9.892	5.408	7.818	19.51	23.26
Ni	13.09	30.16	21.66	21.35	16.99	13.36	203.7	92.12
Cu	13.75	145.0	11.75	5.258	3.290	39.98	116.1	31.08
Zn	667.2	917.2	1152	565.3	356.1	509.0	2813	802.8
Rb	64.30	n.d.	110.1	37.09	33.01	98.58	n.d.	n.d.
Sr	20.53	n.d.	37.64	29.52	22.23	26.77	n.d.	n.d.
Y	2.353	n.d.	6.950	7.995	1.978	5.975	n.d.	252.5
Zr	102.2	815.3	45.20	96.98	49.59	69.09	753.3	81.08
Nb	8.305	109.4	11.11	6.624	4.621	6.651	107.7	8.901
La	2.611	225.0	21.60	39.54	24.65	5.687	135.5	189.8
Ce	10.01	230.1	35.67	31.92	30.04	36.12	317.5	470.0
Pr	0.949	28.89	2.228	3.491	2.080	3.105	28.53	51.70
Nd	3.039	86.40	6.696	6.338	5.378	6.982	95.78	232.2
Sm	1.215	18.38	1.676	1.516	1.025	1.462	16.52	50.50
Eu	0.251	3.915	0.396	0.344	0.412	0.397	3.959	9.739
Gd	1.345	19.25	1.810	1.815	2.231	1.680	13.72	51.62
Tb	0.076	2.815	0.156	0.171	0.132	0.194	2.260	6.975
Dy	0.528	13.08	0.681	0.917	0.799	1.103	11.52	41.13
Ho	0.096	2.438	0.112	0.158	0.165	0.295	2.025	8.040
Er	0.349	6.805	0.615	0.672	0.325	1.464	6.355	21.69
Tm	0.064	1.035	0.175	0.142	0.097	0.081	0.892	2.941
Yb	0.993	7.294	0.605	2.990	0.565	1.147	6.755	17.11
Lu	0.048	0.868	0.075	0.138	0.058	0.094	0.822	2.320
Hf	1.267	19.44	1.336	1.110	1.116	1.156	14.78	2.105
Ta	0.262	6.132	0.573	0.306	0.327	0.397	6.939	0.619
W	0.577	12.77	1.763	0.994	1.056	1.078	14.94	0.812
Pb	19.35	2413	39.11	14.42	23.80	27.14	838.6	21.19
Th	1.755	98.68	3.639	2.732	2.211	4.555	106.4	24.15
U	1.455	37.37	2.080	1.896	1.788	2.619	32.68	4.197

	Lommel Maatheide						
	2A-LOM6	2B-LOM1	2B-LOM2	2B-LOM3	2B-LOM4	2B-LOM5	2B-LOM6
P	115.8	296.2	231.7	644.8	760.2	861.6	362.0
S	353.2	291.7	410.4	8498	23131	19570	174.7
Sc	51.00	17.85	20.49	34.34	50.58	14.93	34.73
Ti	2125	4549	1430	5769	4531	1861	1401
V	119.7	167.9	61.14	68.82	111.7	226.9	74.44
Cr	71.00	114.7	37.80	311.1	358.0	481.8	32.81
Mn	102.5	107.3	61.67	169.1	177.1	357.5	58.48
Co	10.16	8.269	11.75	17.99	25.82	26.96	9.578
Ni	22.90	18.25	16.29	47.13	51.96	68.87	14.25
Cu	27.17	17.47	8.098	28.26	36.86	28.83	10.56
Zn	1145	293.1	2735	27422	592.7	1125	347.0
Rb	n.d.	189.7	137.3	n.d.	n.d.	n.d.	147.8
Sr	n.d.	66.28	38.34	n.d.	n.d.	n.d.	36.43
Y	n.d.	17.95	13.41	n.d.	n.d.	n.d.	6.083
Zr	129.1	1035	394.1	224.9	641.5	190.5	299.6
Nb	27.85	33.47	17.29	17.85	16.08	17.39	19.73
La	137.0	17.74	12.73	153.1	407.7	645.9	11.60
Ce	70.86	137.9	81.79	142.8	347.4	605.6	76.63

Continued

Table 3. Continued

	Lommel Maatheide						
	2A-LOM6	2B-LOM1	2B-LOM2	2B-LOM3	2B-LOM4	2B-LOM5	2B-LOM6
Pr	5.409	7.405	5.394	14.81	42.52	75.05	3.255
Nd	25.54	23.29	11.19	65.23	179.6	335.4	14.66
Sm	4.934	6.150	3.478	16.31	47.65	86.61	2.265
Eu	0.888	1.304	0.825	3.251	9.359	16.94	0.537
Gd	4.139	1.939	1.988	15.77	48.04	111.1	2.808
Tb	0.441	0.740	0.417	2.349	7.877	14.98	0.340
Dy	1.681	4.597	2.546	12.99	41.90	71.91	1.650
Ho	0.383	0.877	0.518	2.449	7.930	14.31	0.307
Er	1.184	4.784	1.279	6.651	20.62	38.52	1.078
Tm	0.191	0.480	0.397	1.007	2.761	5.412	0.294
Yb	1.802	4.479	2.407	6.521	17.78	33.50	1.545
Lu	0.138	0.497	0.213	0.783	2.263	4.164	0.140
Hf	3.278	27.64	11.46	6.220	23.06	5.825	7.241
Ta	1.601	2.320	1.095	1.890	1.595	1.123	0.828
W	4.401	6.859	3.349	1.971	1.271	0.576	2.555
Pb	73.25	125.8	69.64	44.41	25.28	17.24	47.42
Th	7.109	12.68	4.293	17.20	29.76	13.94	4.036
U	4.869	12.07	5.450	4.411	5.777	1.711	4.376

The following isotopes were monitored during the analytical runs: P^{31}, S^{34}, Sc^{45}, Ti^{47}, V^{51}, Cr^{53}, Mn^{55}, Fe^{57}, Co^{59}, Ni^{60}, Cu^{65}, Zn^{66}, Rb^{85}, Sr^{88}, Y^{89}, La^{139}, Ce^{140}, Pr^{141}, Nd^{143}, Sm^{147}, Eu^{153}, Gd^{157}, Tb^{159}, Dy^{163}, Ho^{165}, Er^{166}, Tm^{169}, Yb^{172}, Lu^{175}, Hf^{178}, Ta^{181}, W^{182}, Pb^{208}, Th^{232}, and U^{238}.
n.d., no data available.

Younger Coversand I (Table 3). The organic-rich part in the Lutterzand sequence represented by sandy peat (LUT-3, LUT-4, and LUT-8-1, 2, 3) is characterized by very high concentrations of S (0.80–4.5%), P (up to 1218 ppm), and Se (10–20 ppm). Organic-rich samples from the Usselo Horizon display higher concentrations of the rare earth elements (REE) than the Younger Coversands I and II (Fig. 6). Such high REE concentrations accompanied by lower concentrations of some other trace elements are pronounced as deep troughs at Nb-Ta, P, Zr-Hf, Ti, and Co-Ni for the Usselo Horizon samples on the ACC-normalized diagram (Fig. 6). The sample LUT-7 from a thin sandy layer just below the peat (Fig. 3) is compositionally most notable. It shows strongly elevated concentrations of S (0.65%), and displays higher concentrations than any other sample of Zr (636 ppm), Ni (298 ppm), Mn (317 ppm), Co (22 ppm), Hf (80 ppm), and Pb (2484 ppb) (Table 1). The sample LUT-7 not only displays somewhat unusual trace element characteristics, but also displays much stronger PGE signals on the ICP-MS spectrum compared with signals for other samples from this and other outcrops (Table 4). Sample LUT-8-1 from the lowermost part of the peat layer (just above the thin sandy layer) displays high concentrations of Pb (2509 ppb), whereas concentrations of other elements are similar to those from the rest of the peat samples.

Lommel Molse-Nete

All samples from this outcrop are characterized by elevated values relative to the ACC concentrations of Rb (167–360 ppm), U (5.3–12.9 ppm), Sc (22–120 ppm), V (168–387 ppm) and W (2.3–7.4 ppm), and lowered concentrations of Sr (36–92 ppm) and Y (5.3–45 ppm) (Table 3). Samples from the Younger Coversands I and II are compositionally similar to each other except for the Younger Coversand II being richer in P, S, Co, Ni, and Zn, and slightly poorer in Ti and Rb (Table 3). Samples 1LOM-1 (the Younger Coversand I) and 1LOM-9 (the Younger Coversand II) display high concentrations of Zr (360 and 580 ppm, respectively) and Hf (10.5 and 10.7 ppm, respectively). Lommel Molse-Nete samples (except those from the Usselo Horizon) display REE concentrations and patterns similar to those of ACC (Fig. 6). On the ACC-normalized diagram, the Usselo Horizon samples stood apart from the rest of the samples (although all studied samples from the Molse-Nete site are represented by sand) because of elevated concentrations of the REE and Zr-Hf relative to other samples (Fig. 7). Additionally, sample 1LOM-7 is enriched in Ni (>200 ppm),

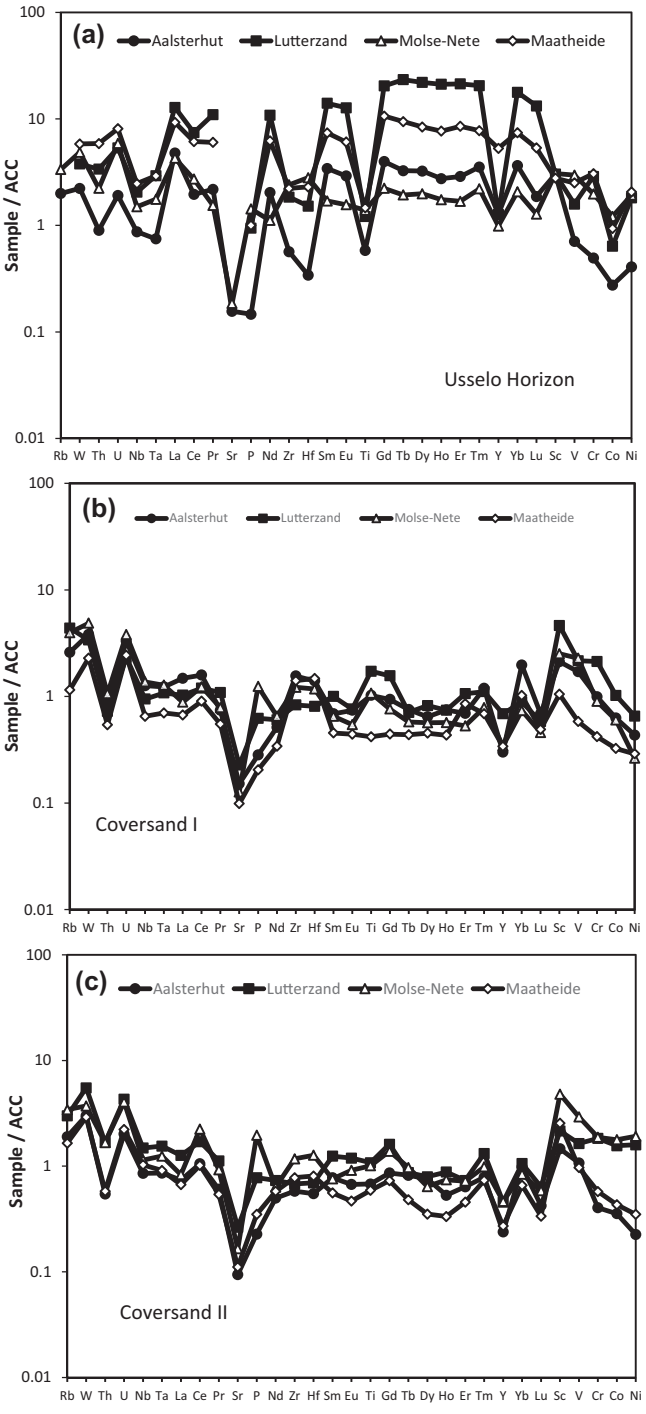

Fig. 6. Averaged ACC-normalized trace element diagrams for the studied sediments (normalizing values are after Wedepohl 1995). (a) Usselo Horizon; (b) Younger Coversand I; (c) Younger Coversand II. Not all analyzed elements are included in this figure for the sake of better representativity.

the concentration of which is comparable to that in sample LUT-7 from Lutterzand (Table 3). Unlike samples from Geldrop-Aalsterhut and Lutterzand, samples from Lommel Molse-Nete do not display troughs at Zr-Hf on the ACC-normalized trace element diagram (Fig. 6). The PGE signals on the ICP-MS spectra for the Lommel Molse-Nete samples are mostly above those for the ACC, with the strongest signals displayed by samples 1LOM-5 and 1LOM-7 (Table 4).

Lommel Maatheide

Samples of the Younger Coversand I from this outcrop are characterized by low concentrations of trace elements, which are generally below the ACC values (Table 3; Fig. 6b) as is overall typical for the Younger Coversand I and II samples studied. A sandy peat layer displays very high concentrations of S (0.85–2.3%) and P (645–1328 ppm), as is typical for similar organic-rich layers from the other studied localities. It also displays much higher concentrations of REE compared with samples of the Younger Coversands I and II, while concentrations of Ta, Nb, P, Zr, Hf, and Ti are comparable to those in the Younger Coversands I and II. This feature is pronounced in troughs in the trace element patterns on the ACC-normalized spider diagrams (Fig. 6). Sample 2A-LOM-4 from a thin sandy layer, the stratigraphic position of which is similar to that of a thin sandy layer from Lutterzand, sample LUT-7 (Figs 3 and 5a), is compositionally distinct from other Lommel Maatheide samples. This sample displays a high concentration of Zn (2813 ppm), Pb (829 ppm), Nb (108 ppm), Ta (6.9 ppm), Zr (>750 ppm), Hf (~15 ppm), Cr (376 ppm), Mn (298 ppm), Co (22 ppm), and Ni (300 ppm) (Table 1). The PGE signal intensities on ICP-MS spectra of the Lommel Maatheide samples are either comparable or somewhat higher than those for Arizona marls (Table 4). Sample 2A-LOM-4 displays a much stronger PGE signal than other samples from the Lommel Maatheide outcrop (Table 4).

Discussion

General features

Various sands (Younger Coversands I and II, and sandy varieties of the Usselo Horizon) represent the main lithology of the studied late Pleistocene samples. The material of the Usselo Horizon was developing in/over already existing sediments during a period before and immediately after the beginning of the Younger Dryas cooling. During the warmer Allerød period, soil formation in the higher and dryer parts of the coversand led to the formation of the Usselo soil horizon, whereas thin peat layers developed in the wetter areas (Kasse 2002; Kaiser *et al.* 2009). All sites sampled include either soil or peat Usselo horizon variety. Overall, the sandy varieties of the Usselo Horizon are similar in geochemical characteristics to the Younger Coversands I and II. However, when the Allerød–Younger Dryas boundary is represented by organic-rich material, a geochemical difference from the sand is clearly observed. This difference is expected and due to the intrinsic lithological differences between the organic-rich and organic-free sediments. However, concentrations and distributions of some trace elements in the sediments studied (see below) are not due completely to the intrinsic characteristics of the sediments, and suggest that a few short events might have affected chemical composition of the sediments. On the basis of the geochemical features observed, we suggest the presence of a possible volcanic component, a component possibly related to biomass burning, and a possible meteoritic component (resulting, for example, from an airbrust/impact episode) in the sediments studied.

Before further discussion, an additional consideration should be made for the Lommel-Maatheide site. Here, a zinc smelter factory was located for a long time that led to severe pollution of soils with heavy metals (e.g. Horckmans *et al.* 2006). The strongest pollution is restricted by the upper 50–60 cm of sediments (sand), but in places, elevated concentrations of the element pollutants can be detected even in samples from the organic-rich Usselo Horizon located as deep as >100 cm from the surface. Only one of the samples studied here (2A-LOM-4) displays strong enrichment in the element pollutants described by Horckmans *et al.* (2006) and also in some other heavy metals (Tables 3 and 4). Such unusually high concentrations of the named elements should be due to contamination by products of the zinc smelter factory. Probably, a thin sandy layer (sample 2A-LOM-4; Fig. 5b) just below the Usselo Horizon peat layer acted as an accumulator of the element pollutants, preventing their further move down the sedimentary sequence. Interestingly enough, sample 2B-LOM-3 collected from the very basis of the Usselo Horizon peat layer (Fig. 5b), although displaying extremely high concentrations of Zn (>2.7%), does not show enrichment in other element pollutants. Therefore, high concentrations of Zn here may be

Table 4. PGE, Re and Au intensities (Cps) for sediments from the Geldrop-Aalsterhut, Lutterzand and Lommel sites (normalized to signal intensities for Murray Springs, AZ marls; see text for details)

	Geldrop-Aalsterhut			Lutterzand						
	AAL-1	AAL-2	AAL-3	LUT-1	LUT-2	LUT-3	LUT-4	LUT-5	LUT-6	LUT-7
Ru	1.03	bdl	1.29	2.45	2.30	bdl	2.61	2.27	3.10	10.02
Rh	1.88	1.11	2.18	2.12	1.38	1.99	11.74	1.18	1.21	8.56
Pd	6.77	2.42	3.67	2.98	5.38	22.20	42.70	2.06	2.56	56.69
Re	2.45	bdl	1.22	9.92	1.35	2.27	2.47	1.08	1.07	4.11
Os	2.04	1.15	bdl	3.98	bdl	bdl	1.64	bdl	bdl	10.70
Ir	1.81	bdl	1.04	4.23	1.09	bdl	3.20	1.07	1.10	10.84
Pt	2.54	bdl	2.74	1.37	1.71	1.26	6.81	bdl	1.37	15.89
Au	5.23	1.63	3.85	8.13	27.85	35.38	42.48	3.60	61.00	23.78

	Lutterzand			Lommel Molse-Nete						
	LUT8-1	LUT8-2	LUT8-3	1LOM-1	1LOM-2	1LOM-3	1LOM-4	1LOM-5	1LOM-6	1LOM-7
Ru	2.97	3.56	3.46	8.94	1.90	1.90	1.87	13.82	6.29	7.37
Rh	7.39	6.45	3.92	1.63	1.19	1.22	1.21	2.97	1.47	3.32
Pd	36.64	22.66	67.15	3.52	1.50	1.59	2.34	4.53	2.93	11.07
Re	9.40	11.93	10.37	1.38	1.40	bdl	bdl	1.62	bdl	4.68
Os	1.40	1.80	1.61	bdl	1.04	bdl	bdl	12.26	bdl	8.69
Ir	1.57	1.93	2.04	1.04	1.43	1.04	1.05	11.19	1.04	11.63
Pt	8.94	2.57	2.88	1.80	1.55	bdl	1.12	3.23	2.01	3.11
Au	22.15	19.00	4.02	2.93	5.12	3.98	1.63	4.33	2.30	9.46

	Lommel Molse-Nete			Lommel Maatheide						
	1LOM-8	1LOM-9	1LOM-10	2LOM-1	2LOM-2	2LOM-3	2A-LOM1	2A-LOM2	2A-LOM3	2A-LOM4
Ru	4.19	3.71	14.93	bdl	2.30	1.54	1.88	bdl	2.60	12.41
Rh	2.02	3.21	1.82	bdl	12.56	bdl	bdl	bdl	1.23	6.82
Pd	2.30	5.06	3.07	bdl	14.08	4.07	1.45	bdl	1.92	9.51
Re	5.70	5.95	4.34	2.38	2.82	bdl	4.09	bdl	5.75	2.54
Os	1.12	1.29	1.66	bdl	1.12	bdl	bdl	bdl	bdl	4.28
Ir	2.58	2.36	3.88	1.05	2.32	1.19	1.09	bdl	1.20	8.85
Pt	1.00	1.75	2.09	bdl	7.71	bdl	bdl	bdl	4.61	6.44
Au	8.20	3.12	6.86	2.54	4.63	55.09	2.93	13.17	28.09	2.04

	Lommel Maatheide							
	2A-LOM5	2A-LOM6	2B-LOM1	2B-LOM2	2B-LOM3	2B-LOM4	2B-LOM5	2B-LOM6
Ru	2.45	1.21	1.81	1.16	2.34	bdl	bdl	1.47
Rh	1.42	2.31	1.20	1.41	bdl	1.56	1.28	1.72
Pd	4.62	2.91	5.91	3.38	12.66	37.56	134.5	2.60
Re	6.58	5.65	4.23	7.14	3.08	7.70	6.65	bdl
Os	1.11	bdl	1.17	bdl	bdl	1.49	bdl	1.62
Ir	1.68	1.16	1.50	1.38	1.05	2.74	1.12	2.19
Pt	1.35	1.63	4.43	5.12	5.56	2.57	1.30	2.59
Au	2.65	1.96	7.34	2.52	4.27	2.80	46.91	3.14

The following isotopes monitored: Ru^{101}, Rh^{103}, Pd^{104}, Pd^{105}, Re^{185}, Os^{189}, Os^{192}, Ir^{193}, Pt^{195} and Au^{196}.
bdl, below the detection limit.

due to the presence of Zn-rich minerals such as sphalerite.

A possible volcanic component in the sediments

Western Europe was volcanically very active in the Late Pleistocene, and more than 30 different tephra layers are recognized in late Glacial sediments alone across Europe (e.g. Vernet *et al.* 1998; Davies *et al.* 2002; Turney *et al.* 2004, 2006; Litt *et al.* 2008; Chapron *et al.* 2012). The presence of a volcanic component in sediments can be identified not only visually by the presence of volcanic glass shards or minerals (as is usually the case), but also on the basis of concentrations of trace elements

such as Nb, Ta, Zr, Hf, Ti, which are common in products of volcanic eruptions ("volcanic" elements) (e.g. Wörner *et al.* 1983; Wastegård *et al.* 2000; Wastegård 2002; Schnurrenberger *et al.* 2003; Kuznetsov and Subetto 2004; Andronikov *et al.* 2014, 2015).

We took a geochemical approach to identify the presence of the volcanic component in the studied sediments. A notable feature displayed by samples LUT-4, LUT-7, LUT-8-1, 8-2, and 8-3 (Lutterzand), 1LOM-5 and 1LOM-7 (Lommel Molse-Nete), and 2LOM-2 and 2A-LOM-4 (Lommel Maatheide) is elevated concentrations of "volcanic" elements such as Nb, Ta, Zr, Hf, Ti, and Pb relative to other samples (Table 3; Fig. 6). Unfortunately, sample 2A-LOM-4 from Lommel-Maatheide is compromised by heavy metal pollution (see above) and is not considered further (Table 3; Fig. 6). For the strongest pollution, the enrichment in volcanic elements is pronounced by a sample LUT-7 (Lutterzand) from a thin sandy layer located just below the organic-rich Usselo Horizon layer (Fig. 3). There are no exact dating results for the sediments enriched in the "volcanic" elements, but the stratigraphic position of such sediments combined with the available age determinations for the sequences studied may correspond to the age of *c*. 12.9 ka BP. It is notable enough that around this time (12 880 cal years BP), the eruption of the Laacher See volcano took place (e.g. Ammann and Lotter 1989; van den Bogaard 1995; Brauer *et al.* 1999; Litt *et al.* 2001, 2008; Riede 2007; Lane *et al.* 2011). During this event, >6 km^3 of magmatic material explosively erupted covering an area of $\sim$1300 km^2 in lava and ash (Wörner and Schmincke 1984; van den Bogaard and Schmincke 1985; van den Bogaard 1995; Schmincke *et al.* 1999; Riede 2007; Litt *et al.* 2008). The studied areas of the Netherlands and Belgium are located away from the main occurrences of the Laacher See tephra (e.g. Riede 2007). However, discoveries of the Laacher See volcanic material in the late Pleistocene sediments of Hautes Fagnes Plateau (East Belgium; Pissart 2003), in fluvial Rhine sediments in the Netherlands (Autin 2008), and potentially as airborne components in sediments from the northern Netherlands (Davies *et al.* 2005) and Sluggan Bog of Northern Ireland (Lowe *et al.* 2004), i.e. in the areas which are also located away from the main occurrences of the Laacher See tephra, indicate transportation of the Laacher See volcanic material away from the main tephra fans. Therefore, it is not unexpected to find the Laacher See volcanic material in sediments of both the Lutterzand and Lommel areas, which are relatively close to the known volcanic plums, as determined by the presence of visible tephra layers. A rough estimate based on the concentrations of Zr and Hf in the Laacher See tephra (Wörner *et al.* 1983) suggests that it would be necessary to add about 10% of the volcanic material to the studied sediments in order to produce an observed change in chemical composition. Later re-deposition of sediments enriched in the volcanic material (not necessarily from the Laacher See volcano eruption alone) may have resulted in the presence of the volcanic signatures in younger sediments from both regions.

A component possibly related to biomass burning

A characteristic feature of samples from the Usselo Horizon in the localities studied is lowered concentrations of some trace elements relative to other trace elements (Fig. 6). This feature is pronounced the most for the organic-rich Usselo Horizon sediments, but to a smaller extent, it is detected for sandy varieties of the Usselo Horizon sediments as well. Therefore, such a feature is not due solely to the presence of the organic component. It is known that most Usselo Horizon lithologies are characterized by the presence of abundant charcoal fragments (e.g. van der Hammen and van Geel 2008; Kaiser *et al.* 2009; van Hoesel *et al.* 2012; present study). It seems reasonable, therefore, to connect at least partly the observed geochemical features of the Usselo Horizon samples with the presence of charcoal. To check this suggestion, we analyzed charcoal fragments from the peat-rich Usselo Horizon in Lutterzand (samples LUT-CH1 and LUT-CH2 of either Allerød or Younger Dryas age), from a podzol of the Allerød (14.07–12.96 ka BP) age (Bertran *et al.* 2009, 2011) in the Landes area of SW France (SWFr-1 and SWFr-2), and from recent wood fires in Arizona, USA (AzF-1, AzF-2, and AzF-3) (Table 5). The paleo-charcoal fragments display concentrations of the REE up to $10\times$ACC, whereas some other trace elements are characterized by much lower concentrations (Table 5), resulting in deep troughs at Zr-Hf and Ta-Nb on the ACC-normalized spider diagram (Fig. 7). Modern charcoal samples display a similar type of trace element distribution, but with much lower concentrations of all trace elements (Table 5; Fig. 7). We cannot yet explain a difference in trace element concentrations between paleo- and modern charcoal samples, but it could be due to the intrinsic features of the source material, i.e. the wood

Table 5. Chemical composition (ppm) of charcoal from Lutterzand (the Netherlands), Landes (SW France) and Arizona (SW USA)

	Lutterzand		SW France		Arizona		
	LUT-CH1	LUT-CH2	SWFr-1	SWFr-2	AzF-1	AzF-2	AzF-3
P	1136	2989	1717	1924	326.2	67.89	119.9
Ti	2300	6017	1183	1868	48.12	24.80	149.4
Cr	234.6	432.4	333.3	406.2	6.294	7.597	9.594
Mn	31.88	48.40	369.1	1992	130.9	31.18	48.19
Co	2.544	6.965	17.17	12.66	1.030	0.232	0.646
Ni	16.31	51.62	99.23	53.55	1.144	0.370	0.804
Y	300.0	613.4	180.1	165.6	11.50	2.942	5.803
Zr	173.9	311.3	45.80	102.2	5.621	2.470	5.140
Nb	10.57	21.25	5.146	10.23	0.971	0.384	0.622
La	430.7	853.2	1647	1283	47.48	9.930	57.03
Ce	385.3	592.9	392.9	388.9	7.727	1.667	3.257
Pr	34.11	95.40	63.72	59.68	2.069	1.077	1.427
Nd	159.4	444.8	247.5	230.2	6.863	3.212	4.771
Sm	40.98	107.0	46.83	44.46	1.606	0.576	0.991
Eu	8.763	21.17	10.21	10.72	0.438	0.154	0.152
Gd	66.15	106.5	41.77	41.60	6.100	1.505	2.202
Tb	8.227	15.68	5.236	5.130	0.424	0.115	0.175
Dy	42.77	93.08	28.91	29.28	1.360	0.387	0.754
Ho	8.509	18.63	5.302	5.314	0.218	0.074	0.134
Er	22.87	51.80	13.41	13.74	0.806	0.171	0.362
Tm	3.028	6.638	1.818	1.961	0.142	0.026	0.063
Yb	18.47	41.30	10.19	11.37	0.701	0.140	0.328
Lu	2.577	5.643	1.237	1.322	0.077	0.014	0.039
Hf	4.640	7.707	1.203	3.061	0.150	0.048	0.130
Ta	1.000	1.620	0.375	0.643	0.041	0.020	0.048
W	1.089	1.569	0.720	0.867	0.017	0.013	0.028
Th	18.05	39.60	34.12	26.12	0.843	0.219	0.537
U	5.287	9.506	8.045	6.632	0.193	0.075	0.162

The following isotopes were monitored: P^{31}, Sc^{45}, Ti^{47}, Cr^{52}, Mn^{55}, Fe^{57}, Co^{59}, Ni^{60}, Y^{89}, Zr^{90}, Nb^{93}, La^{139}, Ce^{140}, Pr^{141}, Nd^{146}, Sm^{147}, Eu^{153}, Gd^{157}, Tb^{159}, Dy^{163}, Ho^{165}, Er^{166}, Tm^{169}, Yb^{172}, Lu^{175}, Hf^{178}, Ta^{181}, W^{182}, Th^{232}, and U^{238}.

characteristics, resulting from differences in soil compositions. It was shown by van Hoesel (2014) that the charring temperature for paleo charcoals from Lutterzand and Lommel is around 420°C, whereas temperatures for charcoal from modern fires are 550–660°C. Maybe the difference in trace element concentrations between paleo charcoal and charcoal from modern fires has something to do with different temperatures of charring. Overall, it is a matter for a separate study. There are no real data on REE compositions of wood material or on most other trace elements. There is also limited information on metallic trace elements, which shows that the concentration of some selected elements can strongly vary for woods from different areas of Europe (e.g. James *et al.* 2014; Füzesi *et al.* 2015; Okmanis *et al.* 2015). It is not surprising, therefore, that the charcoal samples separated not only regionally but also temporally display different trace element compositions. Nevertheless, both paleo and modern charcoal samples display overall similar types of trace element distributions, i.e. deep troughs at Nb-Ta, Zr-Hf, P (except for one modern charcoal sample), and Ti (Fig. 7). It is notable and interesting that the trace element distribution in the charcoal samples is similar for most features to that of the late Pleistocene Usselo Horizon bulk samples (Fig. 6a), although concentrations of trace elements are different for different individual samples. Observed similarities in trace element distributions of charcoal samples and bulk samples from the Usselo Horizon are consistent with the suggestion about geochemical features of the Usselo Horizon due, at least partly, to the presence of charcoal fragments. Generation of charcoal was due to extensive biomass burning. Such biomass burning could be related to the abundance of fuel due to climate change (e.g. van der Hammen and van Geel 2008). Daniau *et al.* (2010) in a study of worldwide charcoal records found that warming climatic events (such as Allerød interstadial) correspond to a peak in products of biomass burning. Fischer *et al.* (2015) made similar observations when studying Greenland ice cores.

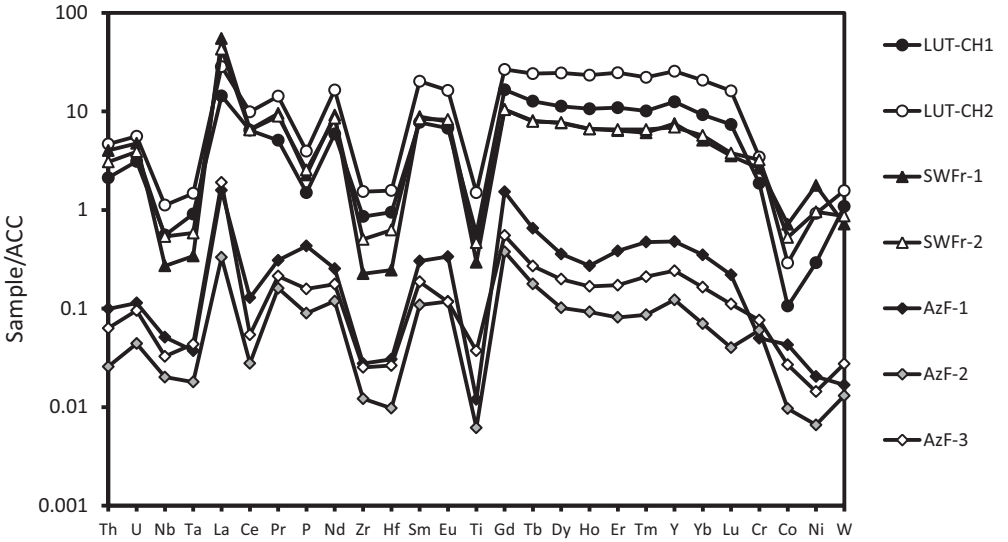

Fig. 7. ACC-normalized trace element diagram for late Pleistocene charcoal samples from the Netherlands and SW France, and modern charcoal samples from southern Arizona (normalizing values are after Wedepohl 1995). Characteristic troughs at Nb-Ta, Zr-Hf, and Ti are distinctly observed for all analyzed samples (see text for more details).

However, such burning occurred 100–200 years after the beginning of warm periods and continued to the early stages of the following cold periods (such as Younger Dryas stadial). Interestingly enough, observations by Fischer *et al.* (2015) show that one of the peaks of biomass burning roughly coincides with the Younger Dryas onset. However, whether this peak is a result of some instantaneous event or just a continuation of the Allerød biomass burning is unclear. The amount of products from biomass burning decreases during the later stages of the cold periods. The available charcoal dates from the Usselo Horizon (Hoek 1997) and recent AMS dates on individual charcoal particles obtained by van Hoesel *et al.* (2012) further suggest that some of the fires must have occurred several hundred years into the Younger Dryas period. These observations fit the suggestions made by Hoek and Bohncke (2002) that wetter conditions during the Allerød could result in the existence of many dead trees, i.e. abundant fuel for wild fires during the earlier stages of the Younger Dryas. All these observations combined suggest that Allerød-Younger Dryas biomass burning was unlikely an instantaneous or short event, but rather took place over an extended period.

However, there is an alternative hypothesis suggesting that simultaneous conflagration happened almost globally *c*. 12.8 ka BP as a response to the meteoritic impact (Firestone *et al.* 2007). However, Artemieva and Morgan (2009), and Morgan *et al.* (2011) showed that although wildfires can ignite as a response to meteoritic impact(s), they would unlikely be ignited globally and mostly in the downrange direction. Recent studies by Svetsov (2008), Daniau (2010), Daniau *et al.* (2010), and Marlon *et al.* (2013) suggest that regional fires caused by small impacts do not differ much from wildfires, which frequently occurred during the late Glacial period either naturally or initiated by humans. Therefore, a reliable tool to distinguish between different types of wild fires still does not exist. We suggest that the presence of signatures of biomass burning in the Usselo Horizon materials could be due to the fires resulting from various causes, which could include a response to the meteoritic impact (either global or local).

A possible meteoritic component in the sediments

Some trace elements are known to present in much higher concentrations in meteorites than in terrestrial materials (e.g. Anders and Grevesse 1989; Wedepohl 1995). Among such "meteoritic" elements, the most informative from the point of view of the presence of the ET component are the PGE (e.g. Sawlowicz 1993; Lorand *et al.* 2008; Palme 2008) because their concentrations in meteorites are about four orders of magnitude higher than in the ACC (450 ppb vs <0.1 ppb,

respectively; Anders and Grevesse 1989; Wedepohl 1995).

A few samples from around the Allerød–Younger Dryas boundary [LUT-7 from a thin sandy layer in Lutterzand (Fig. 3) and, to a lesser extent, 1LOM5 and 1LOM-7 from the lower part of the sandy variety of the Usselo Horizon in Lommel Molse-Nete (Fig. 4)] are enriched in such "meteoritic" elements as Cr, Co, and Ni (Table 3). Additionally, these samples display much stronger PGE signals on the ICP-MS spectra than other samples (Table 4), suggesting some level of PGE enrichment (cf. Petaev *et al.* 2013). The influence of terrestrial processes can explain enrichment in any of the "meteoritic" elements alone (including some PGE; e.g. Sawlowicz 1993). However, simultaneous enrichment in several of these elements should raise suspicion about the potential presence of an ET-related component. The above-named samples from Lutterzand and Lommel display simultaneous enrichment in a few "meteoritic" elements that is consistent with the presence of a meteoritic component. There are no age determinations for these three samples, but according to chronostratigraphic schemes for the regions (Bateman and van Huissteden 1999; Bateman 2008; Derese *et al.* 2012; Vandenberghe *et al.* 2013), these sediments may have been deposited *c*. 12.9 ka BP, which is close to the time of the suggested ET event (Firestone *et al.* 2007). However, whether the presence of the meteoritic component in the sediments studied is due to long-term enrichment through meteoritic rain, a local meteorite shower, or some much wider-pronounced event still remains unclear.

Conclusions

A study of the late Pleistocene sediments from the Netherlands and Belgium has shown that some geochemical features of the sediments studied could not be explained by the intrinsic characteristics of sediments only. Geochemical characteristics of samples from around the Allerød–Younger Dryas boundary in NW Europe point to a sharp change in conditions of sedimentation just before the onset of the Younger Dryas cooling event (*c*. 12.8 ka BP). One such feature, which is found in samples from the Usselo Horizon, is deep troughs at Zr-Hf and Ta-Nb on the ACC-normalized diagram. A similar but more strongly pronounced distribution is displayed by the charcoal samples. We tentatively relate this feature to the presence of abundant charcoal fragments resulting from extensive biomass burning. This biomass burning was most likely due to the abundant fuel, generated as a response to change in climatic conditions. Although these wildfires likely ignited because of terrestrial causes, a relation to an ET event (local, regional, or global) cannot be excluded. Another geochemical feature was identified in a thin sandy layer at the base of the Allerød to Younger Dryas peat layer. This sandy layer combines geochemical signatures of the volcanic and the meteoritic materials, and in a few cases displays a "charcoal-like" distribution of trace elements. That is, the sediments experienced the addition of compositionally anomalous materials during a short event *c*. 12.9 ka BP. We tentatively connect enrichment in the volcanic elements with the eruption of the Laacher See volcano (12.88 ka BP) according to the stratigraphic position of such sediments. The presence of a possible meteoritic component in the same sediments suggests that an ET event occurred at approximately the same time. However, whether the presence of the meteoritic component is due to a local meteorite impact/airburst or to a much stronger event remains unclear. Anyway, it is quite possible that some short and dramatic event took place just before the onset of the Younger Dryas climate oscillation, but, as was emphasized by Haynes *et al.* (2010), an understanding of what happened at *c*. 12.9–12.8 ka BP requires further research.

Since the suggested unusual events might have taken place over a narrow time frame, it is difficult to apply absolute age determinations precisely. It seems to be more practical to use relative stratigraphic positions of sediment layers displaying anomalous geochemical characteristics and restricted by time frames estimated on the basis of absolute age determinations to correlate such layers over the extended territory.

Acknowledgements

The authors thank D.S. Lauretta for the opportunity to work in his cosmochemistry laboratory, and R.J. Maxwell for help during fieldwork. They thank C.V. Haynes Jr, J. Ballenger, M. Drury, C. Verbruggen, N. van den Putten, D. Subetto, and E. Rudnickaitė for very fruitful discussions on the issues considered. They also thank P. Bertran for providing the late Pleistocene samples from France. F. Geerts, M. van Gils, and B. Vanmontfort are thanked for help with work at the Lommel outcrops. The authors are very grateful to two anonymous reviewers for careful reading of the manuscript

and for invaluable comments and suggestions. J. Zucarelly (nee Alley) is thanked for help with editing. This study was supported in part by the NAI International Collaboration Fund for AVA.

Alexandre V. Andronikov, Czech Geological Survey, Geologicka 6, 15200 Prague 5, Czech Republic
*E-mail:*alexandre.andronikov@geology.cz

Annalies Van Hoesel, Leiden University, Faculty of Archaeology, Einsteinweg 2, NL-2333 CC Leiden, The Netherlands
*E-mail:*vanhoesel.geo@gmail.com

Irina E. Andronikova, Czech Geological Survey, Geologicka 6, 15200, Prague 5, Czech Republic
*E-mail:*irina.andronikova@geology.cz

Wim Z. Hoek, Utrecht University, Faculty of Geoscience, Heidelberglaan 2, NL-3584 CS Utrecht, The Netherlands
*E-mail:*w.z.hoek@uu.nl

References

Alley, R.B., 2000. The Younger Dryas cold interval as viewed from central Greenland. *Quaternary Science Review*, 19, 213–226.

Ammann, B. and Lotter, A.F., 1989. Late-Glacial radiocarbon- and palynostratigraphy on the Swiss Plateau. *Boreas*, 18, 109–126.

Anders, E. and Grevesse, N., 1989. Abundances of the elements: meteoritic and solar. *Geochimica et Cosmochimica Acta*, 53, 197–214.

Andronikov, A.V., Lauretta, D.S., Connolly, Jr H.C. and Andronikova, I.E., 2013. Determination of trace-element bulk composition of equilibrated ordinary chondrite meteorite samples by LA-ICP-MS using various reference materials. In: *44th Lunar and Planetary Science Conferences*. Lunar and Planetary Institute Contribution No. 1719.

Andronikov, A.V., Rudnickaitė, E., Lauretta, D.S., Andronikova, I.E., Kaminskas, D., Šinkūnas, P. and Melešytė, M., 2015. Geochemical evidence of the presence of volcanic and meteoritic materials in Late Pleistocene lake sediments of Lithuania. *Quaternary International*, 386, 18–29.

Andronikov, A.V., Subetto, D.A., Lauretta, D.S., Andronikova, I.E., Drosenko, D.A., Kuznetsov, D.D., Sapelko, T.V. and Syrykh, L.V., 2014. In search for fingerprints of an extraterrestrial event: trace element characteristics of sediments from the lake Medvedevskoye (Karelian Isthmus, Russia). *Doklady Earth Sciences*, 457, 818–822.

Artemieva, N. and Morgan, J., 2009. Modeling the formation of the K-Pg boundary layer. *Icarus*, 201, 768–780.

Autin, W.J., 2008. Stratigraphic analysis and paleoenvironmental implications of the Wijchen Member in the lower Rhine-Meuse Valley of the Netherlands. *Netherlands Journal of Geosciences*, 87, 291–307.

Bateman, M.D., 2008. Luminescence dating of periglacial sediments and structures. *Boreas*, 37, 574–588.

Bateman, M.D. and van Huissteden, J., 1999. The timing of last-glacial periglacial and aeolian events, Twente, eastern Netherlands. *Journal of Quaternary Science*, 14, 277–283.

Berger, W.H., 1990. The Younger Dryas cold spell – a quest for causes. *Global and Planetary Change*, 3, 219–237.

Bertran, P., Allenet, G., Ge, T., Naughton, F., Poirier, P. and Sanchez Goni, M.F., 2009. Coversand and Pleistocene paleosols in the Landes region, southwestern France. *Journal of Quaternary Science*, 24, 259–269.

Bertran, P., Bateman, M.D., Hernandez, M., Mercier, N., Millet, D., Sitzia, L. and Tastet, J.-P., 2011. Inland aeolian deposits of south-west France: facies, stratigraphy and chronology. *Journal of Quaternary Science*, 26, 374–388.

Björck, S., 2007. Younger Dryas oscillation, global evidence. In: Scott, A.E. (ed.), *Encyclopedia of Quaternary Science*. Elsevier, Oxford. 1983–1995.

Brauer, A., Enders, C. and Negendank, J.F.W., 1999. Lateglacial calendar year chronology based on annually laminated sediments from Lake Meerfelder Maar, Germany. *Quaternary International*, 61, 17–25.

Brauer, A., Haug, G.H., Dulski, P., Sigman, D.M. and Negendank, J.F.W., 2008. An abrupt wind shift in Western Europe at the onset of the Younger Dryas cold period. *Nature Geoscience*, 1, 520–523.

Bunch, T.E., Hermes, R. E., Moore, A.M.T., Kennett, D.J., Weaver, J.C., Wittke, J.H., DeCarli, P.S., Bischoff, J.L., Hillman, G.C., Howard, G.A., Kimbel, D.R., Kletetschka, G., Lipo, C.P., Sakai, S., Revay, Z., West, A., Firestone, R.B. and Kennett, J.P., 2012. Very high-temperature impact melt products as evidence for cosmic airbursts and impacts 12,900 years ago. *Proceedings of the National Academy of Science*, 109, 1903–1912.

Chapron, E., Ledoux, G., Simonneau, A., Albéric, P., St-Onge, G., Lajeunesse, P. and Boivin, P., 2012. New evidence of Holocene mass wasting events in recent volcanic lakes from the French Massif Central (lakes Pavin, Montcineyre and Chauvet) and implications for natural hazards. *Advances in Natural and Technological Hazards Research*, 31, 255–264.

Daniau, A.-L., 2010. Global patterns of biomass burning during the last glacial period. *PAGES News*, 18, 61–63.

Daniau, A.-L., Harrison, S.P. and Bartlein, P.J., 2010. Fire regimes during the Last Glacial. *Quaternary Science Reviews*, 29, 2918–2930.

Davies, S.M., Branch, N.P., Lowe, J.J. and Turney, C.S.M., 2002. Towards a European tephrochronological framework for Termination 1 and the Early Holocene. *Philosophical Transactions of the Royal Society of London*, A360, 767–802.

Davies, S.M., Hoek, W.Z., Bohncke, S.J.P., Lowe, J.J., Pyne O'Donnell, S. and Turney, C.S.M., 2005. Detection of Late-glacial distal tephra layers in the Netherlands. *Boreas*, 34, 123–135.

Derese, C., Vandenberghe, D.A.G., van Gils, M., Mees, F., Paulissen, E. and van den Haute, P., 2012. Final Palaeolitic settlements of the Campine region (NE Belgium) in their environmental context: optical age constraints. *Quaternary International*, 251, 7–21.

De Vries, H., Barendsen, G.W. and Waterbolk, H.T., 1958. Groningen radiocarbon dates II. *Science*, 127, 129–137.

Firestone, R.B., West, A., Kennett, J.P., Bunch, T.E., Revay, Z.S., Schultz, P.H., Belgya, T., Kennett, D.J.,

Erlandson, J.M., Dickenson, O.J., Goodyear, A.C., Harris, R.S., Howard, G.A., Kloosterman, J.B., Lechler, P., Mayewski, P.A., Montgomery, J., Poreda, R., Darrah, T., Que Hee, S.S., Smith, A.R., Stich, A., Topping, W., Wittke, J.H. and Wolbach, W.S., 2007. Evidence for an extraterrestrial impact 12,900 years ago that contributed to the megafaunal extinctions at the Younger Dryas cooling. *Proceedings of the National Academy of Science*, 104, 16016–16021.

Fischer, H., Schüpbach, S., Gfeller, G., Bigler, M., Röthlisberger, R., Erhardt, T., Stocker, T.F., Mulvaney, R. and Wolff, E., 2015. Millennial changes in North American wildfire and soil activity over the last glacial cycle. *Nature Geoscience*, 8, 723–727.

Füzesi, I., Heil, B. and Kovacs, G. 2015. Effects of wood ash on the chemical properties of soil and crop vitality in small plot experiments. *Acta Sylvatica and Lignaria Hungarica*, 11, 55–64.

Haynes, C.V., Jr, Boerner, J., Domanik, K., Lauretta, D., Ballenger, J. and Goreva, J., 2010. The Murray Spring Clovis site, Pleistocene extinction, and the question of extraterrestrial impact. *Proceedings of the National Academy of Science*, 107, 4010–4015.

Hijszeler, C.C.W.J., 1957. Late-glacial human cultures in the Netherlands. *Geologie en Mijnbouw*, 19, 288–302.

Hoek, W.Z. 1997. Late-Glacial and early Holocene climatic events and chronology of vegetation development in the Netherlands. *Vegetation History and Archaeobotany*, 6, 197–213.

Hoek, W.Z. and Bohncke, S.J.P., 2002. Climatic and environmental events over the Last Termination, as recorded in the Netherlands: a review. *Netherlands Journal of Geosciences*, 81, 123–137.

Horckmans, L., Swennen, R. and Deckers, J., 2006. Geochemical and mineralogical study of a site severely polluted with heavy metals (Maatheide, Lommel, Belgium). *Environmental Geology*, 50, 725–742.

Israde-Alcántara, I., Bischoff, J.L., Domíniguez-Vásquez, G., Li, H.-C., DeCarli, P.S., Bunch, T.E., Wittke, J.H., Weaver, J.C., Firestone, R.B., West, A., Kennett, J.P., Mercer, C., Xie, S., Richman, E.K., Kinzie, C.R. and Wolbach, W.S., 2012. Evidence from Central Mexico supporting the Younger Dryas extraterrestrial impact hypothesis. *Proceedings of the National Academy of Science*, 109, E738–E747.

James, A.K., Helle, S.S., Thring, R.W., Sarohia, G.S. and Rutherford, P.M., 2014. Characterization of inorganic elements in woody biomass bottom ash from a fixed-bed combustion system, a downdraft gasifier and a wood pellet burner by fractionation. *Energy and Environment Research*, 4, 85–94.

Jochum, K.P., Weis, U., Stoll, B., Kuzmin, D., Yang, Q., Raczek, I., Jacob, D.E., Stracke, A., Birbaum, K., Frick, D.A., Günther, D. and Enzweiler, J., 2011. Determination of reference values for NIST SRM 610–617 glasses following ISO guidelines. *Geostandard and Geoanalytical Research*, 35, 397–429.

Kaiser, K., Hilgers, A., Schlaak, N., Jankowski, M., Kühn, P., Bussemer, S. and Przegietka, K., 2009. Palaeopedological marker horizons in northern central Europe: characteristics of Lateglacial Usselo and Finow soils. *Boreas*, 38, 591–609.

Kasse, C., 2002. Sandy aeolian deposits and environments and their relation to climate during the Last Glacial Maximum and Lateglacial in northwest and central Europe. *Progress in Physical Geography*, 26, 507–532.

Kennett, J.P., Kennett, D.J., Culleton, B.J., Aura Tortosa, J.E., Bischoff, J.L., Bunch, T.E., Daniel, I.R. Jr, Erlandson, J.M., Ferraro, D., Firestone, R.B., Goodyear, R.C., Israde-Alcántara, I., Johnson, J.R., Jorda Pardo, J.F., Kimbel, D.R., LeCompte, M.A., Lopinot, N.H., Mahaney, W.C., Moore, A.M., Moore, C.R., Ray, J.H., Stafford, T.W. Jr, Tankersley, K.B., Wittke, J.H., Wolbach, W.S. and West, A., 2015. Bayesian chronological analyses consistent with synchronous age of 12,835-12,735 Cal B.P. for Younger Dryas boundary on four continents. *Proceedings of the National Academy of Science*, 112, E4344–E4353.

Kuznetsov, D.D. and Subetto, D.A., 2004. Tephrochronology and its application to paleolimnology. *Reports of the Russian Geographic Society*, 134, 79–82. [In Russian]

Lane, C.S., Blockley, S.P.E. and Lotter, A.F., 2011. Tephrochronology and absolute centennial scale synchronisation of European and Greenland records for the last glacial to interglacial transition: a case study of Soppensee and NGRIP. *Quaternary International*, 246, 145–156.

Litt, T., Brauer, A., Goslar, T., Merkt, J., Balaga, K., Müller, H., Ralska-Jasiewiczowa, M., Stebich, M. and Negendank, J.F.W., 2001. Correlation and synchronisation of Late-glacial continental sequences in northern central Europe based on annually laminated lacustrine sediments. *Quaternary Science Reviews*, 20, 1233–1249.

Litt, T., Schmincke, H.-U., Frechen, M. and Schlüchter, C., 2008. Quaternary. In: McCann, T. (ed.), *Geology of Central Europe Volume 2: Mesozoic and Cenozoic*. Geological Society Publishing House, London. 1287–1340.

Lorand, J.-P., Lufuet, A. and Alard, O., 2008. Platinum-group elements: a new set of key tracers for the Earth's interior. *Elements*, 4, 247–252.

Lowe, J.J., Rasmussen, S.O., Björck, S., Hoek, W.Z., Steffensen, J.P., Walker, M.J.C., Yu, Z.C. and INTIMATE Group, 2008. Synchronisation of palaeoenvironmental events in the North Atlantic region during the Last Termination: a revised protocol recommended by the INTIMATE group. *Quaternary Science Reviews*, 27, 6–17.

Lowe, J.J., Walker, M.J.C., Scott, E.M., Harkness, D.D., Bryant, C.L. and Davies, S.M., 2004. A coherent high-precision radiocarbon chronology for the Late-glacial sequence at Sluggan Bog, Co. Antrim, Northern Ireland. *Journal of Quaternary Science*, 19, 147–158.

Marlon, J.R., Bartlein, P.J., Daniau, A.L., Harrison, S.P., Maezumi, S.Y., Power, M.J., Tinner, W. and Vanniere, B., 2013. Global biomass burning: a synthesis and review of Holocene paleofire records and their controls, *Quaternary Science Reviews*, 65, 5–25.

McManus, J.F., Francois, R., Gherardi, J.-M., Keigwin, L.D. and Brown-Legar, S., 2004. Collapse and rapid resumption of Atlantic meridional circulation linked to deglacial climate changes. *Nature*, 428, 834–837.

Morgan, J., Artemieva, N., Belcher, C., Goldin, T. and Pierazzo, E., 2011. Revisiting fires at the K-Pg boundary. *Meteoritics and Planetary Science*, 46, A166.

Muhs, D.R., Budahn, J., Avila, A., Skipp, G., Freeman, J. and Patterson, D., 2010. The role of African dust in the formation of Quaternary soils on Mallorca, Spain and implications for the genesis of Red Mediterranean soils. *Quaternary Science Reviews*, 29, 2518–2543.

Murton, J.B., Bateman, M.D., Dallimore, S.R., Teller, J.T. and Yang, Z., 2010. Identification of Younger Dryas outburst flood path from Lake Agassiz to the Arctic Ocean. *Nature*, 464, 740–743.

Okmanis, M., Lazdina, D. and Lazdinš, A., 2015. The composition and use value of tree biomass ash. *Rural Sustainability Research*, 34, 32–37.

Palme, H., 2008. Platinum-group elements in cosmochemistry. *Element*, 4, 233–238.

Petaev, M.I., Huang, S., Jacobsen, S.B. and Zindler, A., 2013. Large Pt anomaly in the Greenland ice points to a cataclysm at the onset of Younger Dryas. *Proceedings of the National Academy of Science*, 110, 12917–12920.

Peteet, D., 1995. Global Younger Dryas? *Quaternary International*, 28, 93–104.

Pinter, N., Scott, A.C., Daulton, T.L., Podoll, A., Koeberl, C., Anderson, R.S. and Ishman, S.E., 2011. The Younger Dryas impact hypothesis: a requiem. *Earth Science Reviews*, 106, 247–264.

Pissart, A., 2003. The remnants of Younger Dryas lithalsas on the Hautes Fagnes Plateau in Belgium and elsewhere in the world. *Geomorphology*, 52, 5–38.

Rayburn, J.A., Cronin, T.M., Franzi, D.A., Knuepfer, P.L.K. and Willard, D.A., 2011. Timing and duration of North American glacial lake discharges and the Younger Dryas climate reversal. *Quaternary Research*, 75, 541–551.

Riede, F., 2007. Der Ausbruch des Laacher See-Vulkans vor 12.920 Jahren und urgeschichtlicher Kulturwande am Ende des Alleroed. Eine neue Hypothese zum Ursprung der Bromme-Kultur und des Purstunien. *Mitteilungen der Gesellschaft fuer Urgeschichte*, 16, 25–54.

Sawlowicz, Z., 1993. Iridium and other platinum-group elements as geochemical markers in sedimentary environments. *Palaeogeography, Palaeoclimatology, Palaeoecology*, 104, 253–270.

Schmincke, H.-U., Park, C. and Harms, E., 1999. Evolution and environmental impact of the eruption of Laacher See Volcano (Germany) 12,900 a BP. *Quaternary International*, 61, 61–72.

Schnurrenberger, D., Russell, J. and Kelts, K., 2003. Classification of lacustrine sediments based on sedimentary components. *Journal of Paleolimnology*, 29, 141–154.

Svetsov, V.S., 2008. Terminal radiation and fires after impacts of cosmic objects. In: Adushkin, V.V. and Nemchinov, I.V. (eds), *Catastrophic Events Caused by Cosmic Objects*. Springer, Berlin. 207–226.

Sylvester, P.J., 2008. Matrix effects in laser ablation-ICP-MS. *Mineralogic Association of Canada Short Course*, 40, 67–78.

Sylvester, P.J. and Eggins, S.M., 1997. Analysis of Re, Au, Pd, Pt and Rh in NIST glass certified reference materials and natural basalt glasses by laser ablation ICP-MS. *Geostandards Newsletter*, 21, 215–229.

Teller, J.T., Leverington, D.W. and Mann, J.D., 2002. Freshwater outbursts to the ocean from glacial Lake Agassiz and their role in climate change during the last deglaciation. *Quaternary Science Reviews*, 21, 879–887.

Tian, H., Schryvers, D. and Clayes, Ph., 2010. Nanodiamonds do not provide unique evidence for a Younger Dryas impact. *Proceedings of the National Academy of Science*, 108, 40–44.

Turney, C.S.M., Lowe, J.J., Davies, S.M., Hall, V., Lowe, D.J., Wastegård, S., Hoek, W.Z., Alloway, B. and SCOTAV and INTIMATE MEMBERS, 2004. Tephrochronology of Last Termination Sequences in Europe: a protocol for improved analytical precision and robust correlation procedures (a joint SCOTAV-INTIMATE proposal). *Journal of Quaternary Science*, 19, 111–120.

Turney, C.S.M., van den Burg, K., Wastegård, S., Davies, S.M., Whitehouse, N.J., Pilcher, J.R. and Callaghan, C., 2006. North European glacial-interglacial transition (LGIT; 15.9 ka) tephrochronology: extended limits and new events. *Journal of Quaternary Science*, 21, 335–345.

Vandenberghe, D.A.G., Derese, C., Kasse, C. and van den Haute, P., 2013. Late Weichselian (fluvio-)aeolian sediments and Holocene drift-sands of the classic type locality in Twente (E Netherlands): a high-resolution dating study using optically stimulated luminescence. *Quaternary Science Reviews*, 68, 96–113.

Van den Bogaard, P., 1995. $^{40}Ar/^{39}Ar$ ages of sanidine phenocrysts from Laacher See Tephra (12,900 yr BP): chronostratigraphic and petrological significance. *Earth and Planetary Science Letters*, 133, 163–174.

Van den Bogaard, P. and Schmincke, H.-U., 1985. Laacher See Tephra: a widespread isochronous Late Quaternary tephra layer in central and northern Europe. *The Geological Society of America Bulletin*, 96, 1554–1571.

Van der Hammen, T. and van Geel, B., 2008. Charcoal in soils of the Allerød-Younger Dryas transition were the result of natural fires and not necessarily the effect of an extraterrestrial impact. *Netherlands Journal of Geosciences*, 87, 359–361.

Van Hoesel, A., 2014. *The Younger Dryas climate change: was it caused by an extraterrestrial impact*? PhD thesis, Utrecht University. *Utrecht Studies in Earth Sciences*, 54.

Van Hoesel, A., Hoek, W., Braatbaard, F., van der Plicht, H., Pennock, J.M. and Drury, M.R., 2012. Nanodiamonds and wildfire evidence in the Usselo horizon postdate the Allerød-Younger Dryas boundary. *Proceedings of the National Academy of Science*, 109, 7648–7653.

Van Hoesel, A., Hoek, W.Z., Pennock, J.M. and Drury, M.R., 2014. The Younger Dryas impact hypothesis: a critical review. *Quaternary Science Reviews*, 83, 95–114.

Van Hoesel, A., Hoek, W.Z., Pennock, G.M., Kaiser, K., Plümper, O., Jankowski, M., Hamers, M.F., Schlaak, N., Küster, M., Andronikov, A.V. and Drury, M.R., 2015. A search for shocked quartz grains in the Allerød–Younger Dryas boundary layer. *Meteoritics and Planetary Science*, 50, 483–498.

Vanmontfort, B., van Gils, M., Paulissen, E., Bastianes, J., de Bie, M. and Meirsman, E., 2010a. Human occupation of the Late and Early Post-Glacial environments in the Liereman Landscape (Campine, Belgium). *Journal of Archaeology in the Low Countries*, 2-2.

Vanmontfort, B., Yperman, W., Lambrechts, B., van Gils, M. and Geerts, F., 2010b. Een finaalpaleolithisch en meslotisch sitecomplex te Lommel, Molste Nete. Opgravingscampagne 2010. *Notae Praehistoricae*, 30, 29–34.

Vernet, G., Raynal, J.P., Fain, J., Miallier, D., Montret, M., Pilleyre, T. and Sanzelle, S., 1998. Tephrostratigraphy of the last 160 ka in Western Limagne (France). *Quaternary International*, 47/48, 139–146.

Wastegård, S., 2002. Early to middle Holocene silicic tephra horizons from the Katla volcanic system, Iceland: New results from Faroe Islands. *Journal of Quaternary Science*, 17, 723–730.

Wastegård, S., Wohlfarth, B., Subetto, D.A. and Sapelko, T.V., 2000. Extending the known distribution of the Younger Dryas Vedde Ash into northwestern Russia. *Journal of Quaternary Science*, 15, 581–586.

Wedepohl, K.H., 1995. The composition of the continental crust. *Geochimica et Cosmochimica Acta*, 59, 1217–1232.

Wittke, J.H., Weaver, J.C., Bunch, T.E., Kennett, J.P., Kennett, D.J., Moore, A.M.T., Hillman, G.C., Tankersley, K.B., Goodyear, A.C., Moore, C.R., Daniel, I.R., Ray, J.H., Lopinot, N.H., Ferraro, D., Israde-Alcántara, I., Bischoff, J.L., DeCarli, P.S., Hermes, R.E., Kloosterman, J.B., Revay, Z., Howard, G.A., Kimbel, D.R., Kletetschka, G., Nabelek, L., Lipo, C.P., Sakai, S., West, A. and Firestone, R.B. 2013. Evidence for deposition of 10 million tonnes of impact spherules across four continents 12,800 y ago. *Proceedings of the National Academy of Sciences*, 110, E2088–E2097.

Wörner, G. and Schmincke, H.-U., 1984. Mineralogical and chemical zonation of the Laacher See Tephra sequence (East Eifel, W. Germany). *Journal of Petrology*, 25, 805–835.

Wörner, G., Beusen, J.-M., Duchateau, N., Gijbels, R. and Schmincke, H.-U., 1983. Trace element abundances and mineral/melt distribution coefficients in phonolites from the Laacher See Volcano (Germany). *Contributions to Mineralogy and Petrology*, 84, 152–173.

